Contents

1. General Experimental Section

All operations were carried out under an atmosphere of nitrogen or argon, unless stated otherwise. Spectrophotometric grade (99.9%) chlorobenzene and benzene were purchased from Alfa Aesar or Sigma-Aldrich and dried over CaH_2, distilled and deoxygenated at least three "freeze-pump-thaw" cycles prior to use. 6,13-Bis-tri(isopropylsilylethynyl)pentacene (≥99%, HPLC) was purchased from Sigma-Aldrich and used as received. $PC_{61}BM$ was purchased from NanoC. The dimeric compounds $(2\text{-Y-DMBI})_2$ were synthesized as described previously.[1] ^1H, ^{13}C, COSY and NOESY NMR spectra were recorded either on a Bruker AMX 400 or 500 MHz spectrometer. Electrochemical measurements were carried out under nitrogen in 0.1 M tetra-*n*-butylammonium hexafluorophosphate in dry tetrahydrofuran, using a CH Instruments CHI620D potentiostat. A conventional three-electrode cell was used, with a glassy carbon working electrode, platinum wire counter electrode, and a Ag wire coated with AgCl as the pseudoreference electrode. Potentials were referenced to ferrocenium/ferrocene by using internal ferrocene, decamethylferrocene, or cobaltocenium hexafluorophosphate. UV measurements were performed on a Varian Cary 5E UV-Vis-NIR spectrometer. All of the samples were prepared in a glove-box at room temperature. The solutions were transferred to a clean 1 mm path length PTFE-stopcock-sealed quartz cuvette (175 – 2700 nm) upon mixing, and the UV-Vis-NIR measurement was started as rapidly as possible. The temperature for the cuvette holder was controlled by a Quantum Northwest TC 125 temperature controller.

2. Discussion of Dimer Synthesis and Characterization

The dimers were obtained, as described in the Supporting Information of Reference [1], through reduction of salts of the corresponding Y-DMBI^+ cations in THF using either 1 wt% Na-Hg or 25 wt% Na-K (CARE – HIGHLY PYROPHORIC). Several 2-aryl-DMBI+ salts were also reduced with Na-Hg, but the presumed dimeric products were less stable and could not be isolated. The corresponding amides (Figure 1) were obtained as side products in some cases. The amides are formed more readily when the Y-DMBI^+ salt is poorly soluble in THF. Thus, reduction of the poorly soluble PF_6^- or BPh_4^- salts of 2-Fc-DMBI^+ and 2-Rc-DMBI^+ afforded amide:dimer ratios as large as 1:1, whereas the more soluble $\text{2-Cyc-DMBI}^+PF_6^-$ gave a ratio of

ca. 1:10. No detectable side-products were formed on reduction of the highly soluble tetrakis(3,5-bis(trifluoromethyl)phenyl)borate (BAr'_4^-) salts of 2-Fc-DMBI$^+$ and 2-Rc-DMBI$^+$.

The dimers were characterized by elemental analysis, electrospray mass spectrometry (which showed formation of the monomeric cation under the ionization conditions), ^{1}H and ^{13}C NMR spectroscopy,[1] and, in two cases (see below) by X-ray crystallography. For each dimer in benzene-d_6, the ^{1}H resonance assigned to the *N*-methyl groups is broad at room temperature at 400 MHz, but sharper at higher temperature; presumably this effect is due to restricted rotation around the central DMBI—DMBI bond or the DMBI—Y bond (Figures S1-S2). In the conformer found in the crystal structure of $(2\text{-Fc-DMBI})_2$ the two DMBI moieties are equivalent, but within each DMBI the two NMe groups are inequivalent; the observed broadening could potentially be accounted for if the rate of interconversion of two such conformers through rotation about the Fc–DMBI bond were relatively slow due to steric hindrance.

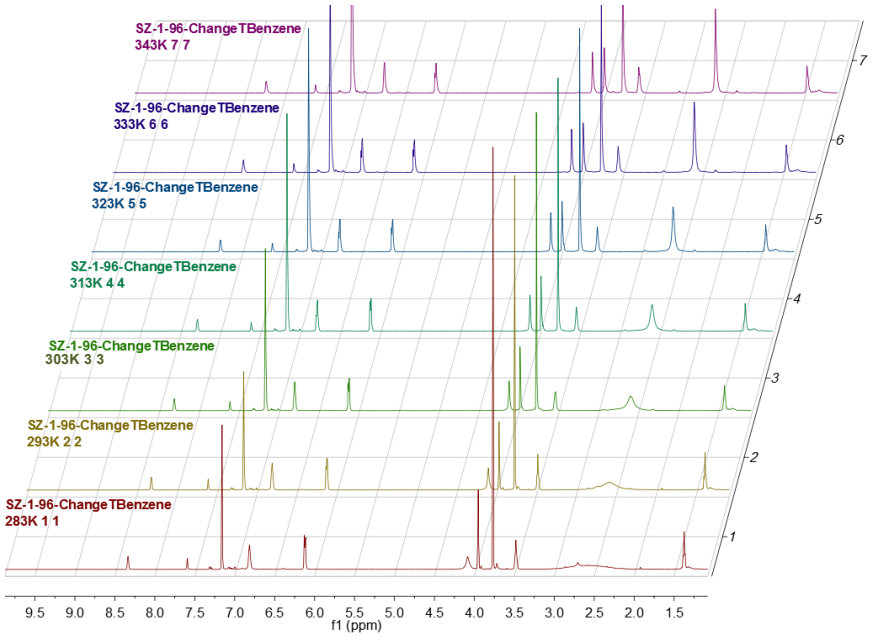

Figure S1. Variable temperature ^{1}H NMR spectra for $(2\text{-Fc-DMBI})_2$ in C_6D_6.

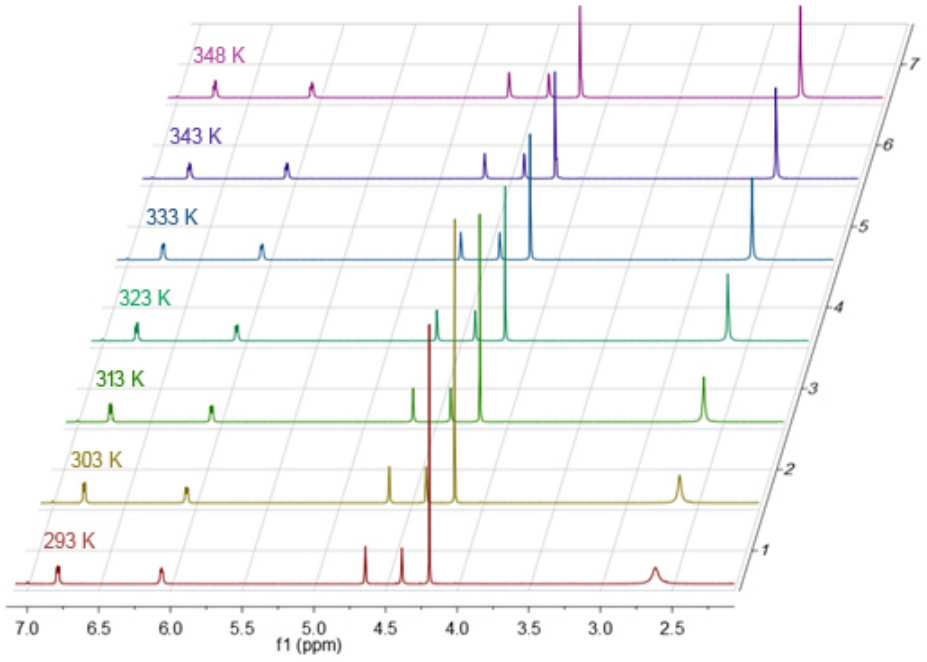

Figure S2. Variable-temperature ^{1}H NMR spectra for (2-Rc-DMBI)$_2$ in C_6D_6.

3. Characterization of DMBI-Derived Amides

In the case of the amide derivative of (2-Cyc-DMBI)$_2$, the amide was synthesized and purified as described below. The structure was confirmed by ^{1}H and ^{13}C NMR spectroscopy, and FT-IR spectroscopy (Figures S3-S5, respectively). The corresponding Fc and Rc derivatives were not isolated, but exhibit similar ^{1}H NMR spectra in solution (when formed by exposing solutions of the appropriate dimer to air and heating to 150 °C) as shown in Figures S6 and S7, respectively, to their Cyc analogue. The metallocenyl derivatives were also characterized by EI-MS, which showed base peaks at *m/z* = 348.1 (M^+) and 394.0 (M^+) for the Fc and Rc amides, respectively.

***N*-Methyl-*N*-(2-(methylamino)phenyl)cyclohexanecarboxamide.** A 20 mL scintillation vial was charged with 39 mg (85 μmol) of (2-Cyc-DMBI)$_2$ and 2 mL of acetone. The solution was sealed under ambient and stirred at 40 ºC for 16 h. The colorless solution turned yellow over the course of the reaction. TLC on SiO_2 with 9:1:0.5, v:v:v, hexanes:ethyl acetate:triethylamine as the eluent indicated complete conversion of the starting material. The solution was concentrated and purified by preparative TLC using the same conditions; the TLC plate solids were extracted with diethyl ether, filtered, and concentrated to yield *N*-methyl-*N*-(2-

(methylamino)phenyl)cyclohexanecarboxamide as a slow-to-crystallize white solid (25 mg, 102 μmol, 60% yield). ^{1}H NMR ($CDCl_3$, 400 MHz): 7.27 (td, J = 7.9, 1.5 Hz, 1H), 6.97 (dd, J = 7.9, 1.5 Hz, 1H), 6.70 (m, overlapping, 2H), 3.85 (br m, 1H), 3.13 (s, 3H), 2.86 (s, 1.5H), 2.85 (s, 1.5H), 2.11 (m, 1H), 1.35-1.7 (m, 7H), 0.85-1.25 (m, 3H); ^{13}C{^{1}H} NMR ($CDCl_3$, 400 MHz): 177.99, 144.92, 129.30, 128.77, 127.67, 116.79, 110.72, 41.10, 35.23, 30.18, 29.51, 25.53, 25.45, 25.40; FT-IR (KBr disc): 3387.2 (N-H), 1647.4 (C=O).

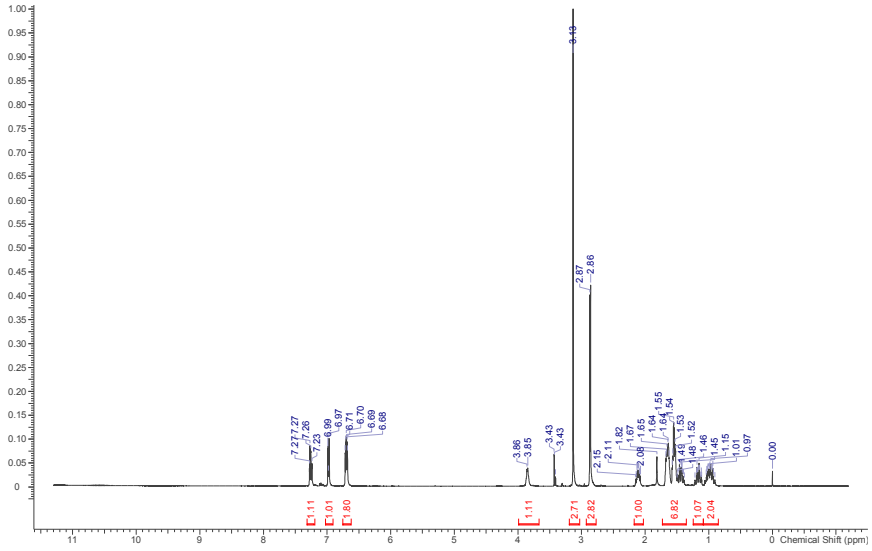

Figure S3. ^{1}H NMR spectrum of the amide derived from (2-Cyc-DMBI)$_2$ in $CDCl_3$.

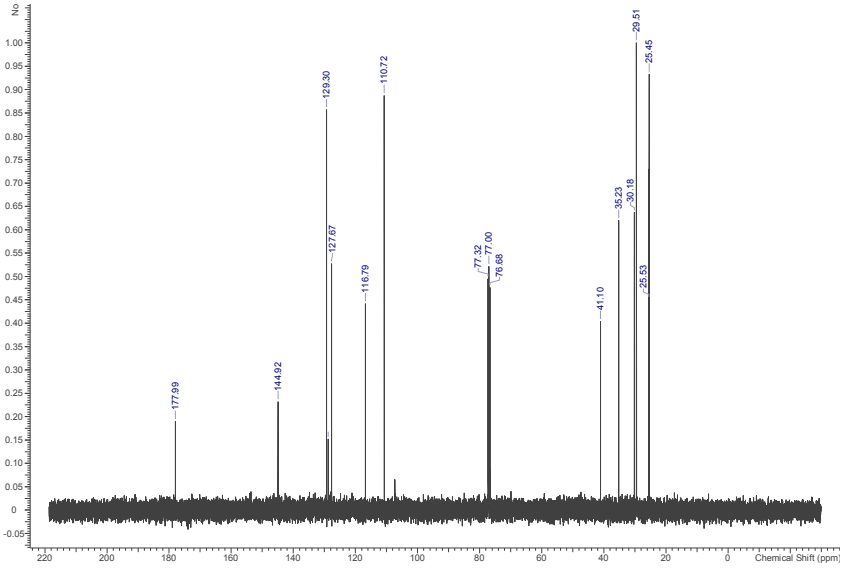

Figure S4. ^{13}C{^{1}H} NMR spectrum of the amide derived from (2-Cyc-DMBI)$_2$ in $CDCl_3$.

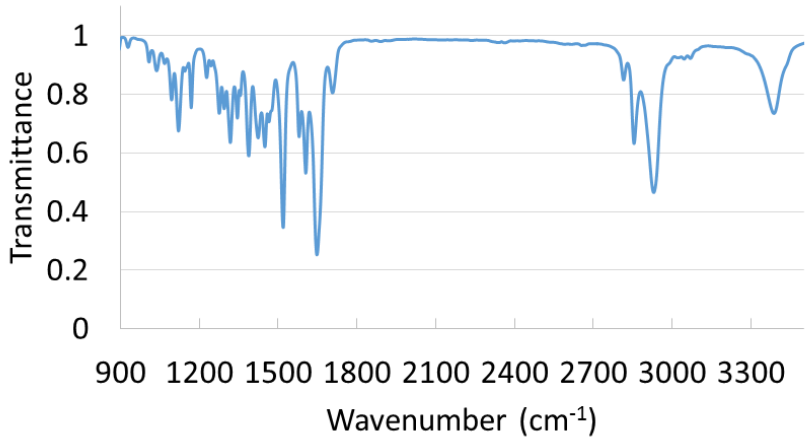

Figure S5. FT-IR spectrum of the amide derived from (2-Cyc-DMBI)$_2$ in a KBr disk.

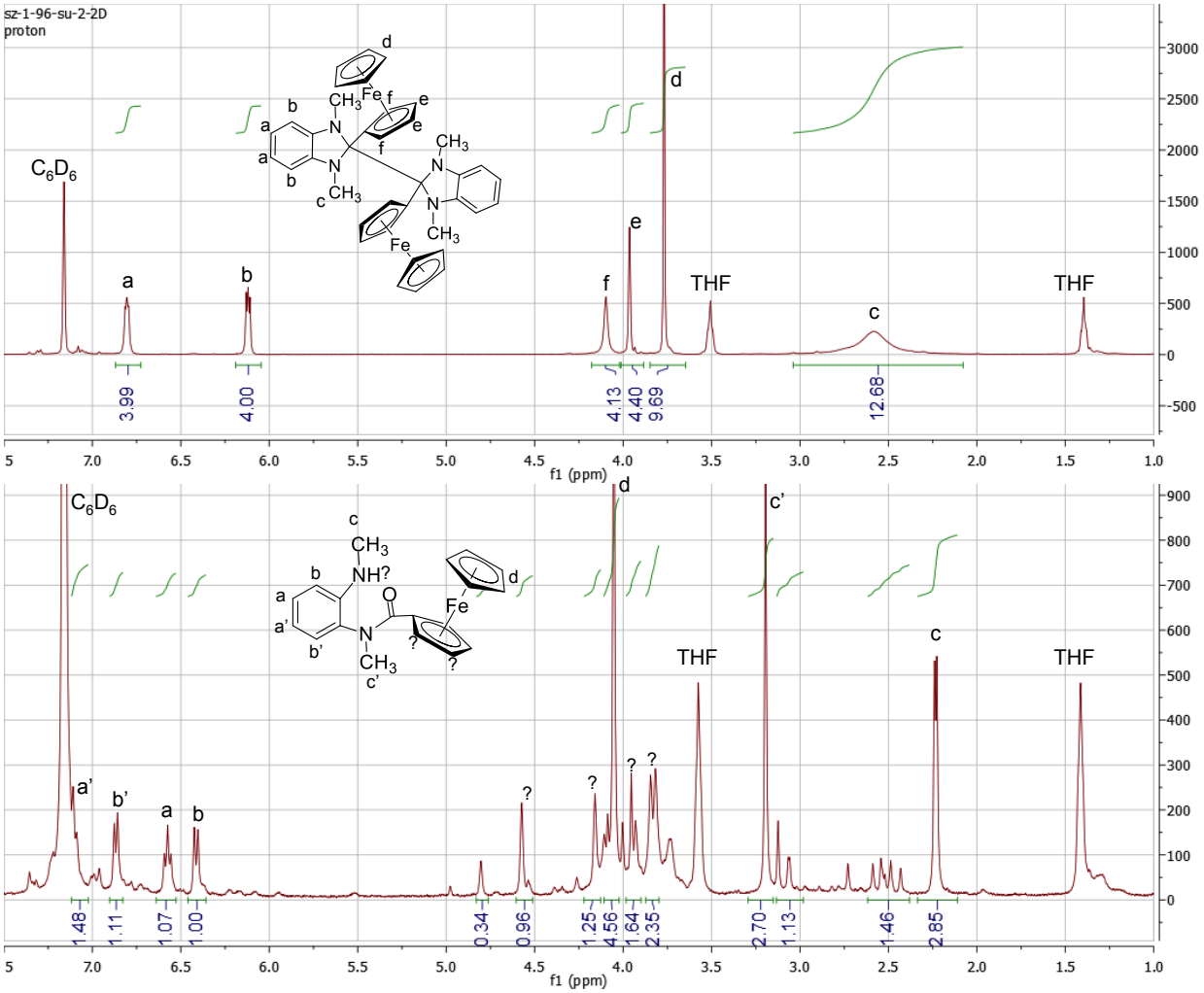

Figure S6. ^{1}H NMR for (2-Fc-DMBI)$_2$ in C_6D_6 (top), and same solution after exposure to air and heating over 150 °C, showing formation of the corresponding amide.

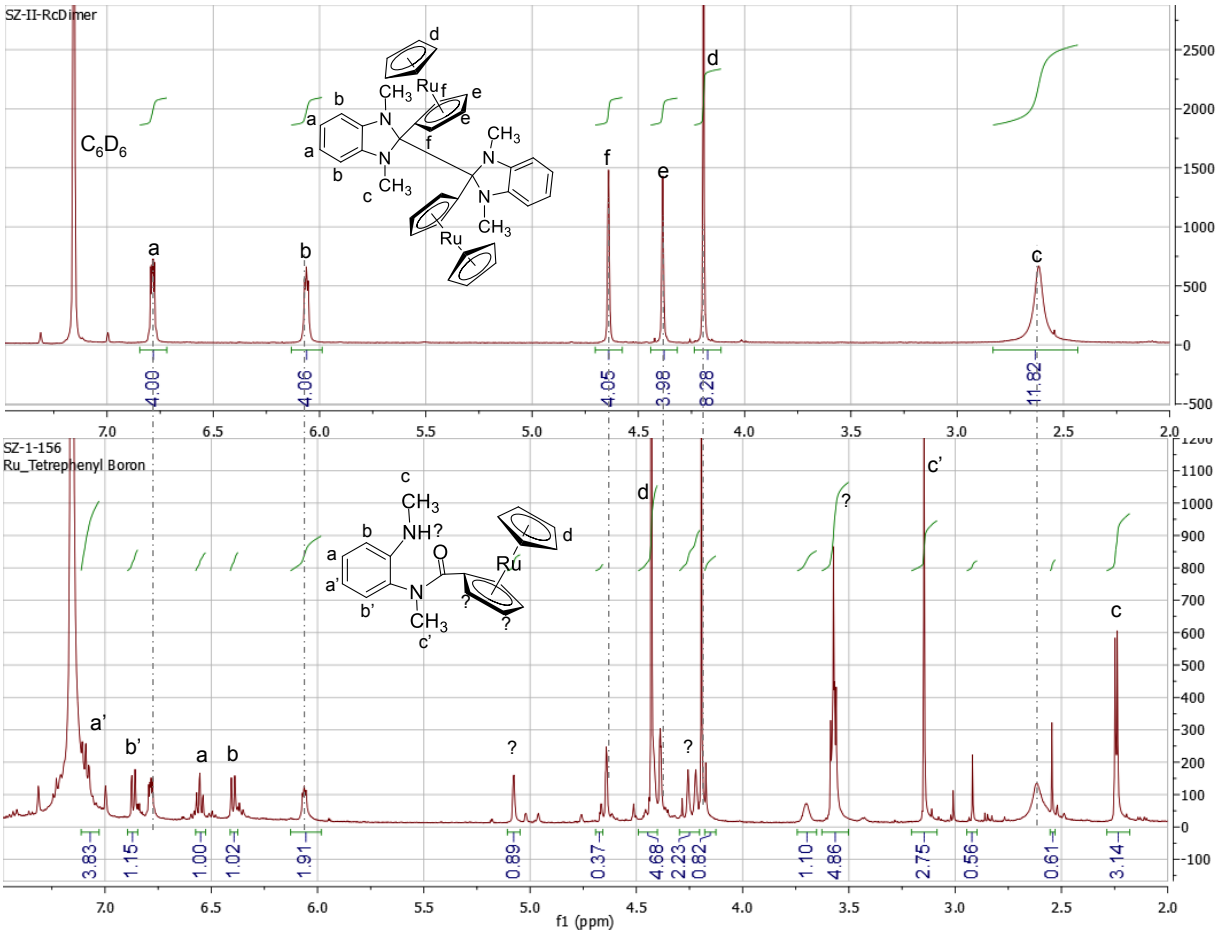

Figure S7. ^{1}H NMR spectrum for (2-Rc-DMBI)$_2$ in C_6D_6 (top), and same solution after exposure to air and heating over 150 °C showing partial conversion to the corresponding amide.

4. Details of Crystal Structure Determinations

Parameters relating to data collection and the structural refinements are summarized below in Table S1. Further details given in CCDC-1048481 ((2-Cyc-DMBI)$_2$) and CCDC-1048482 ((2-Fc-DMBI)$_2$); these data can be obtained free of charge from The Cambridge Crystallographic Data Centre via www.ccdc.cam.ac.uk/data_ request/cif.

Table S1. Selected Crystal and Refinement Parameters for the Crystal Structure Determinations

	(2-Cyc-DMBI)$_2$	(2-Fc-DMBI)$_2$
Crystal growth	Hexane, –20 °C	Layering C_6D_6 solution with heptane
Crystal appearance	Colorless slab	Orange plate
Crystal size / mm^3	0.18 × 0.10 × 0.08	0.20 × 0.10 × 0.05
Empirical formula	$C_{30}H_{42}N_4$	$C_{38}H_{38}Fe_2N_4$
FW	458.67	662.42
Diffractometer	Bruker-Nonius X8 CCD	Bruker APEX-II CCD
λ / Å	1.54178	0.71073
T / K	150[a]	100
Crystal System	Trigonal	Triclinic
Space group	$P3_221$	$P\overline{1}$
a / Å	10.8746(15)	9.893(4)
b / Å	10.8746(15)	11.047(4)
c / Å	19.181(4)	13.583(5)
α / °	90	80.276(5)
β / °	90	87.345(5)
γ / °	120	85.280(5)
V / Å^3	1964.4(7)	1457.4(10)
Z	3	2
ρ(calcd) / Mg m^{-3}	1.163	1.510
μ / mm^{-1}	0.522	1.032
F(000)	750	836
θ range for data / °	4.70-68.39	4.17-25.00
Index ranges	$-11 \le h \le 13$	$-11 \le h \le 11$
	$-13 \le k \le 10$	$-13 \le k \le 13$
	$-18 \le l \le 23$	$-16 \le l \le 16$
Reflections collected	24907	11384
Independent reflection (R_{int})	2404 (0.0372)	5084 (0.0246)
Reflections with $I > 2\sigma(I)$	2357	4450
T_{min}, T_{max}	0.859, 0.942	0.6645, 0.7460
Data / restraints / parameters	2404 / 0 / 156	5084 / 0 / 401
Goodness-of-fit on F^2	1.041	0.999
Final $R1$, $wR2$ [$I > 2s(I)$]	0.0383, 0.1045	0.0339, 0.0863
Final $R1$, $wR2$ (all data)	0.0389, 0.1053	0.0399, 0.0896
Largest peak and hole / e Å^{-3}	0.235, –0.213	0.403, –0.367

[a] At temperatures below ~125K, additional diffuse diffraction was observed, consistent with a reduction of symmetry. On warming these extra spots disappeared, and were completely gone at 150K.

5. Computational Details

All calculations were performed with the Gaussian 09 (Revision B.01) software suite.[2] Geometry optimizations of neutral and cationic states for the monomers and dimers were carried out via density functional theory (DFT) with the M06 functional[3] and the 6-31G(d,p) and LANL2DZ basis sets for the first-row atoms and transition-metal atoms, respectively. The tendency of DFT methods to lead to artificial over-delocalization of odd-electron systems is a known problem for the description of mixed-valence-like systems,[4] of which the adiabatic minima of the dimer radical cations can be considered as examples. Accordingly, care should be taken not to over-interpret the relaxed geometries of the dimer cations or the energies of processes involving these relaxed geometries (adiabatic IEs of dimers, dissociation energies of dimer radical cations).

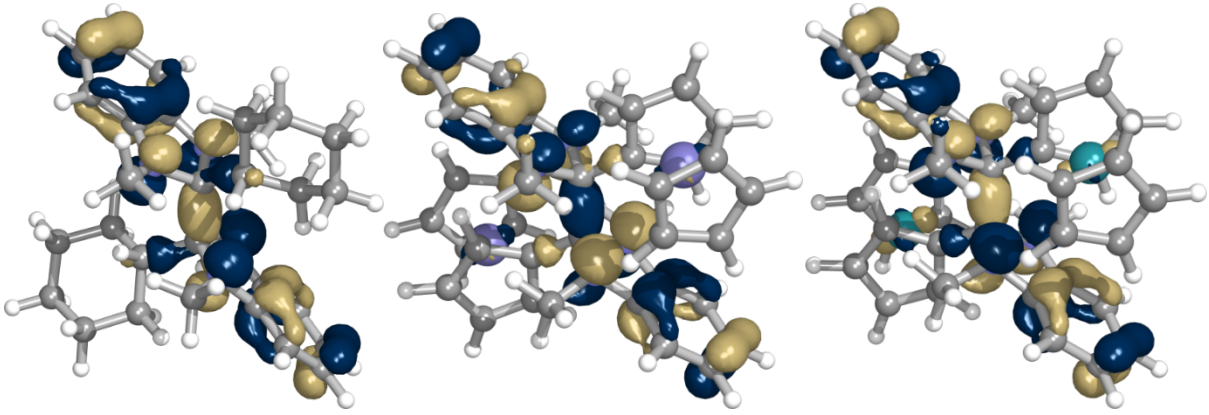

Figure S8. Highest occupied molecular orbitals for (2-Y-DMBI)$_2$ species with, from left to right, Y = Cyc, Fc, and Rc.

6. Cyclic Voltammograms for (2-Y-DMBI)$_2$ and their Corresponding Salts

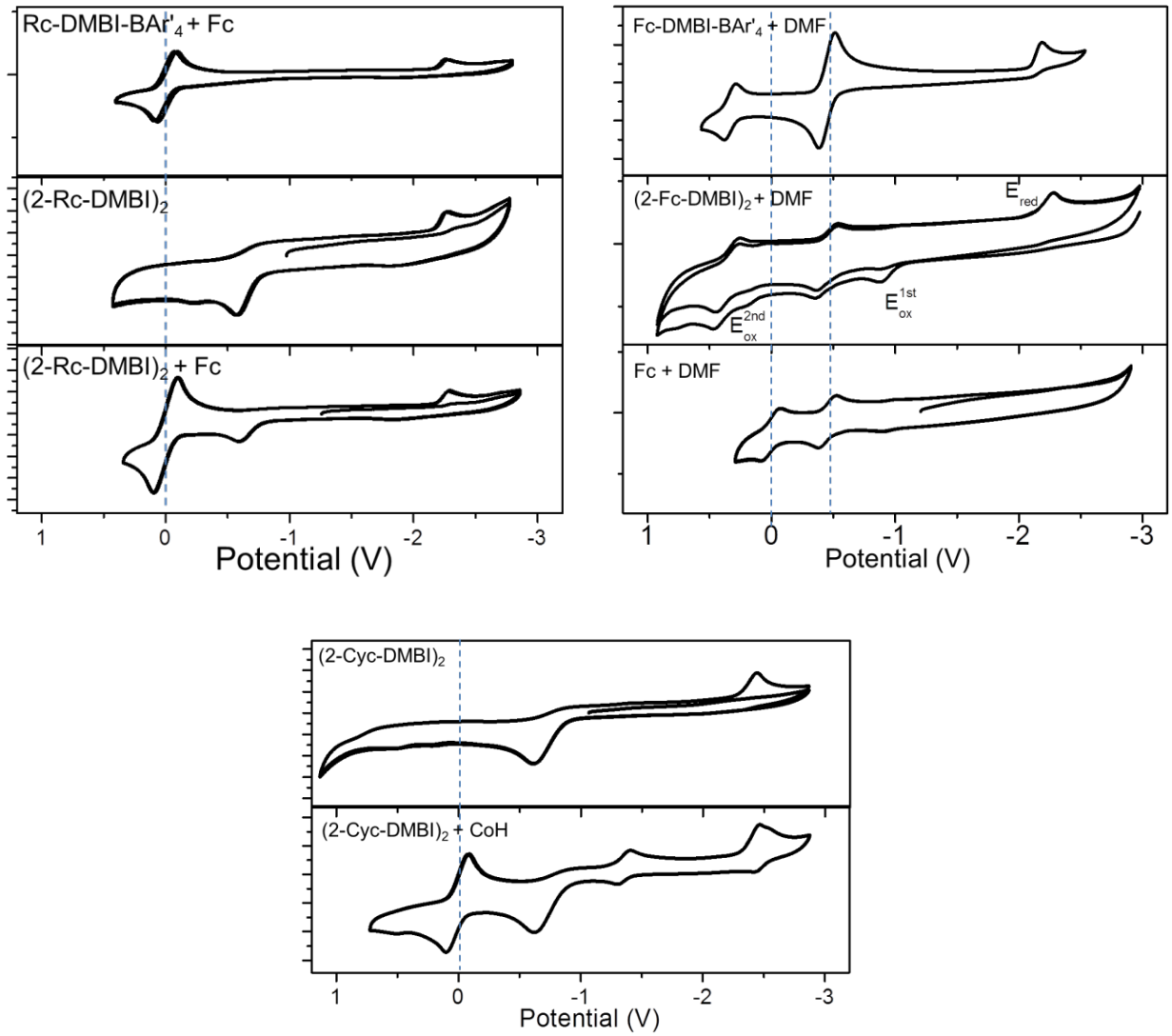

Figure S9. Cyclic voltammograms (100 mV s^{-1}, THF, 0.1 M nBu_4NPF_6, vs. ferrocenium/ferrocene) recorded for 2-Y-DMBI$^+$BAr'$_4^-$ and (2-Y-DMBI)$_2$. DMF, CoH, and Fc denote decamethylferrocene, cobaltocenium hexafluorophosphate, and ferrocene respectively, which are used as internal references.

7. ESR Studies of Dimer Dissociation

Solutions of the pure dimers (ca. 1 mM) in chlorobenzene were investigated in quartz ESR tubes using a X-band Bruker ESR spectrometer operating at 9.44 GHz with a Bruker SHQ cavity. As noted above, only (2-Fc-DMBI)$_2$ showed a signal at room temperature. This spectrum was

consistent with that simulated with WINSIM[5] for 2-Fc-DMBI$^{\bullet}$ using the DFT-derived Isotropic Fermi contact coupling constants given in Table S2, convoluted with a linewidth of 0.45 G.[6]

Table S2. DFT Isotropic Fermi Contact Couplings Used to Simulate the ESR Spectrum of 2-Fc-DMBI$^{\bullet}$.[a]

Nuclei	I	number	A / G
N	1	2	+1.19
$H_{(methyl)}$	$^1/_2$	6	+1.17
$H_{(benzoimid.\ 4,7\text{-positions})}$	$^1/_2$	2	–1.79
$H_{(benzoimid.\ 5,6\text{-positions})}$	$^1/_2$	2	–0.88
$H_{(Fc\ 2,5\text{-positions})}$	$^1/_2$	2	–1.26
$H_{(Fc\ 3,4\text{-positions})}$	$^1/_2$	2	+0.28
$H_{(Fc\ Cp)}$	$^1/_2$	5	–0.12

[a] Isotropic Fermi contact couplings were calculated for the DFT-minimized conformation of the radical. Values of A for chemically equivalent nuclei were then averaged to obtain the values given here.

ΔH_{diss} was then determined by measuring spectra as a function of temperature. In general:

$$-\frac{\Delta H_{diss}}{RT}+\frac{\Delta S_{diss}}{R}=\ln K_{diss}=\ln\frac{[D^{\bullet}]^2}{[D_2]} \qquad \text{(S1)}$$

The ESR intensity, I_{ESR} (either obtained from double integration of the 1st derivative spectrum, or if, as in the present case, the lineshape is invariant with temperature, from the peak-to-peak height in the 1st derivative spectrum) is proportional to [D$^{\bullet}$] and inversely proportional to temperature. Moreover, if the extent of dissociation is small, [D_2] can be regarded as a constant. Thus:

$$\ln\left[I_{ESR}T\right]=-\frac{\Delta H_{diss}}{2RT}+c \qquad \text{(S2)}$$

where c is constant, allowing ΔH_{diss} to be obtained from a plot of the logarithm of the product of intensity and temperature vs. the reciprocal temperature. To determine ΔG_{diss} and ΔS_{diss}, [D$^{\bullet}$] was

determined to be 0.97 μM by comparison of the intensity at 320 K, obtained by double integration of the 1st derivative spectrum, of a sample of known initial [D_2] concentration (1.96 mM) to that of a sample of a solution in chlorobenzene of the stable nitroxyl radical (2,2,6,6-tetramethylpiperidin-1-yl)oxyl (TEMPO) at the same temperature.

8. General Rate Law for Mechanism I

The rate can most generally be expressed as:

$$\frac{d[\mathrm{D}_2]}{dt} = -\frac{1}{2}\frac{d[\mathrm{A}]}{dt} = -\frac{1}{2}k_2[\mathrm{D}^\bullet][\mathrm{A}] \tag{S3}$$

The rate of change of the monomer concentration can be expressed as:

$$\frac{d[\mathrm{D}^\bullet]}{dt} = -2k_{-1}[\mathrm{D}^\bullet]^2 - k_2[\mathrm{D}^\bullet][\mathrm{A}] + 2k_1[\mathrm{D}_2] \tag{S4}$$

Treating $D^\bullet$ as a reactive intermediate and applying the steady state approximation, i.e. setting this rate of change equal to zero, we obtain a quadratic equation in [$D^\bullet$] with roots:

$$[\mathrm{D}^\bullet] = \frac{1 \pm \sqrt{1 + \dfrac{16k_1k_{-1}[\mathrm{D}_2]}{k_2^2[\mathrm{A}]^2}}}{\dfrac{-4k_{-1}}{k_2[\mathrm{A}]}} \tag{S5}$$

and so a rather complicated general rate law of the form:

$$\frac{d[\mathrm{D}_2]}{dt} = -k_2[\mathrm{A}]\left(\frac{1 \pm \sqrt{1 + \dfrac{16k_1k_{-1}[\mathrm{D}_2]}{k_2^2[\mathrm{A}]^2}}}{\dfrac{-4k_{-1}}{k_2[\mathrm{A}]}}\right) \tag{S6}$$

In the case where the first step is rapid, the second step is rate-determining, k_2[A] is small compared to k_{-1}, and as k_2[A]/ k_{-1} tends to vanishing:

$$1 \pm \sqrt{1 + \frac{16k_1k_{-1}[\mathrm{D}_2]}{k_2^2[\mathrm{A}]^2}} \approx \sqrt{\frac{16k_1k_{-1}[\mathrm{D}_2]}{k_2^2[\mathrm{A}]^2}} = \frac{4\sqrt{k_1k_{-1}[\mathrm{D}_2]}}{k_2[\mathrm{A}]} \tag{S7}$$

and

$$[\mathrm{D}^{\bullet}] \approx \sqrt{\frac{k_1[\mathrm{D}_2]}{k_{-1}}} = \sqrt{K_{\mathrm{diss}}[\mathrm{D}_2]} \tag{S8}$$

which, on substituting into Eq. S3 gives Eq. 4 in the main body of the paper. The same result can also be obtained be assuming a pre-equilibrium between D_2 and $D^{\bullet}$.

In the other extreme, where the first step is rate-determining, we can take advantage of the fact that

$$(1+x)^n = 1 + nx + \frac{n(n-1)x^2}{2!} + \frac{n(n-1)(n-2)x^3}{3!} + \ldots \tag{S9}$$

and that for $x << 1$, the terms containing higher powers of x will be small and so:

$$(1+x)^n \approx 1 + nx \tag{S10}$$

which, in our case ($k_2[\mathrm{A}] >> k_{-1}$) means that:

$$[\mathrm{D}^{\bullet}] \approx \frac{1 \pm \left(1 + \frac{8k_1k_{-1}[\mathrm{D}_2]}{k_2^2[\mathrm{A}]^2}\right)}{\frac{-4k_{-1}}{k_2[\mathrm{A}]}} \tag{S11}$$

the positive solution of which can be further simplified to:

$$[\mathrm{D}^{\bullet}] \approx \frac{2k_1[\mathrm{D}_2]}{k_2[\mathrm{A}]} \tag{S12}$$

Substitution into Eq. S3 leads to cancelation of the $k_2[\mathrm{A}]$ terms and to the rate law given for mechanism I in Table 1.

9. Additional Vis-NIR Kinetic Data

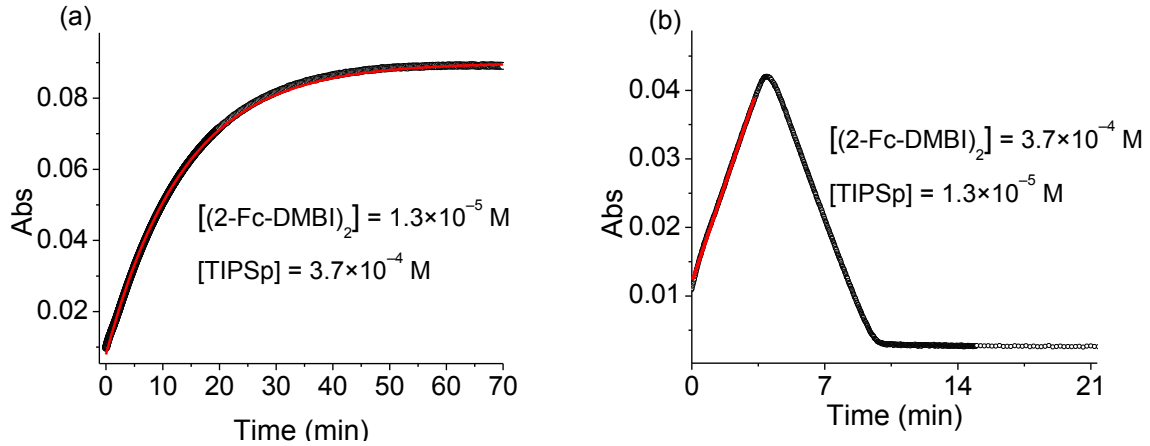

Figure S10. (a) Absorbance at 745 nm vs. time for the reaction of TIPSp and $(2\text{-Fc-DMBI})_2$, when $(2\text{-Fc-DMBI})_2$ is the limiting reagent. The solid red line is the fitted first-order reaction curve. (b) Absorbance at 745 nm vs. time for the same reaction with TIPSp as the limiting reagent. The solid red line is the fitted zero-order reaction curve.

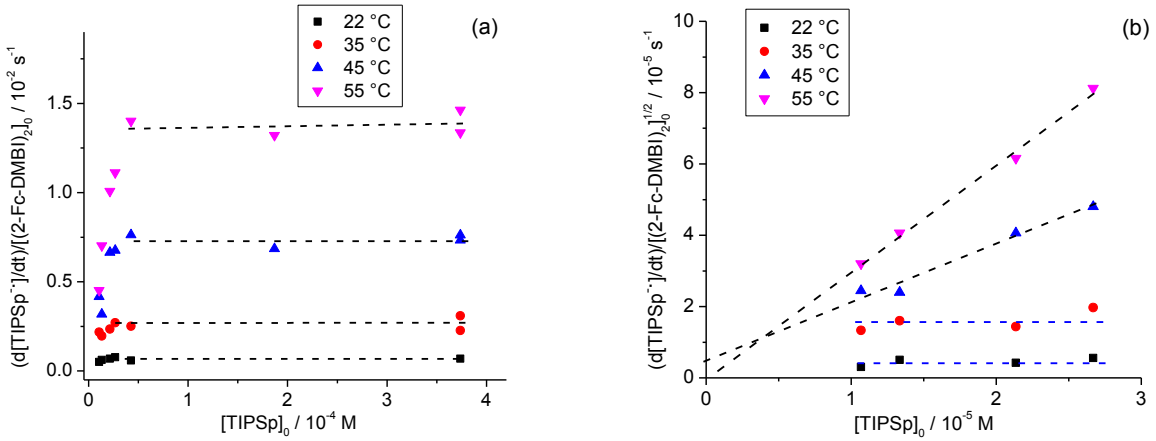

Figure S11. (a) Plots of initial rate divided by the square root of initial concentration of $(2\text{-Fc-DMBI})_2$ versus the initial concentration of acceptor TIPSp, and (b) linear fits at low TIPSp concentration.

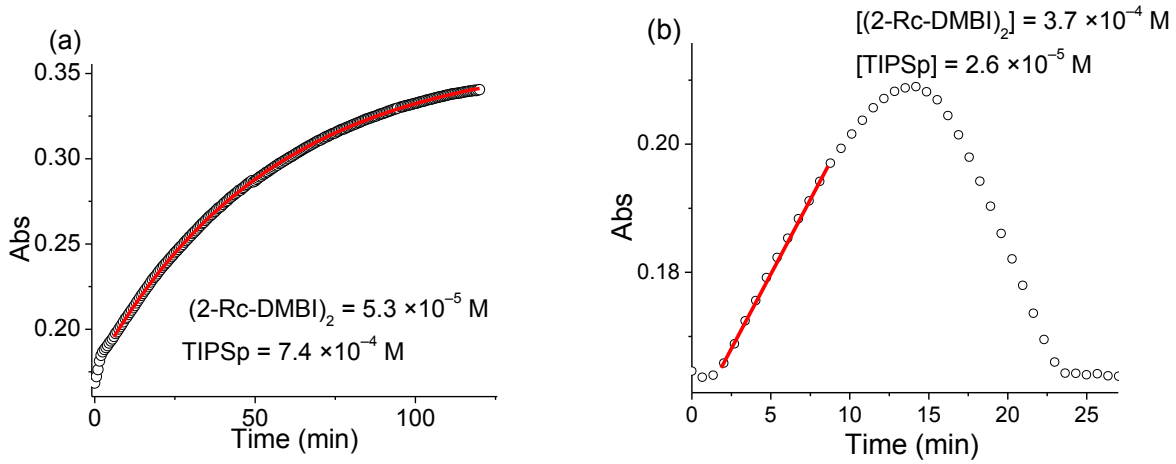

Figure S12. (a) Absorbance at 745 nm vs. time for the reaction of TIPSp and $(2\text{-Rc-DMBI})_2$ with $(2\text{-Rc-DMBI})_2$ as the limiting reagent. The solid red line is the fitted first-order reaction curve. (b) Absorbance at 745 nm vs. time for the same reaction with TIPSp as the limiting reagent. The solid red line is the fitted zero-order reaction curve.

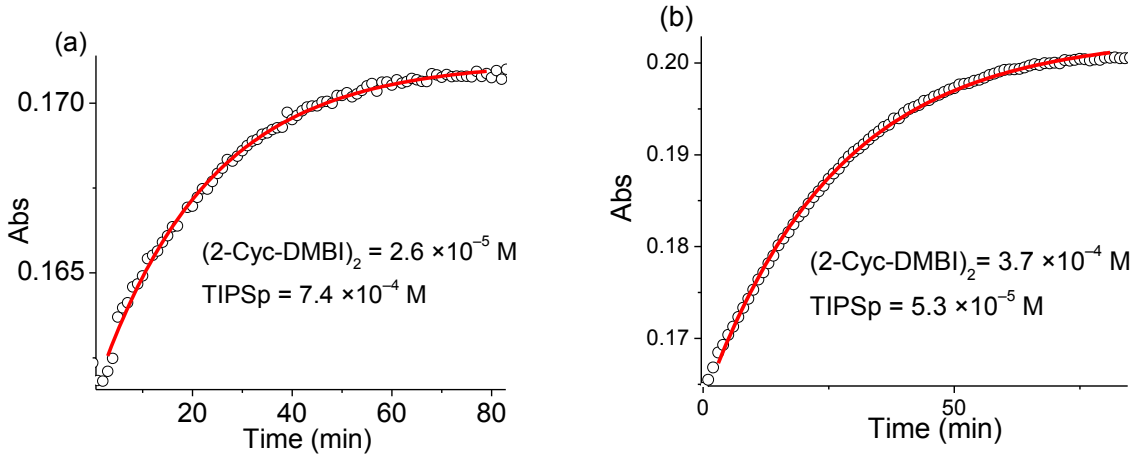

Figure S13. (a) Absorbance at 745 nm vs. time for the reaction of TIPSp and $(2\text{-Cyc-DMBI})_2$, when $(2\text{-Cyc-DMBI})_2$ is the limiting reagent. The solid red line is the fitted first-order reaction curve. (b) Absorbance at 745 nm vs. time for the same reaction with TIPSp as the limiting reagent. The solid red line is the fitted first-order reaction curve.

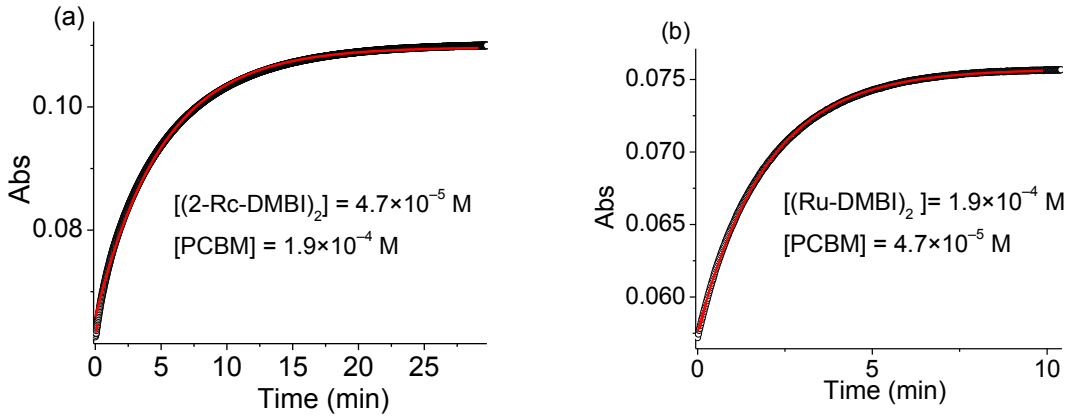

Figure S14. (a) Absorbance at 745 nm vs. time for the reaction of PCBM and (2-Rc-DMBI)$_2$,with (2-Rc-DMBI)$_2$ as the limiting reagent. The solid red line is the fitted first-order reaction curve. (b) Absorbance at 745 nm vs. time for the same reaction with PCBM as the limiting reagent. The solid red line is the fitted first-order reaction curve.

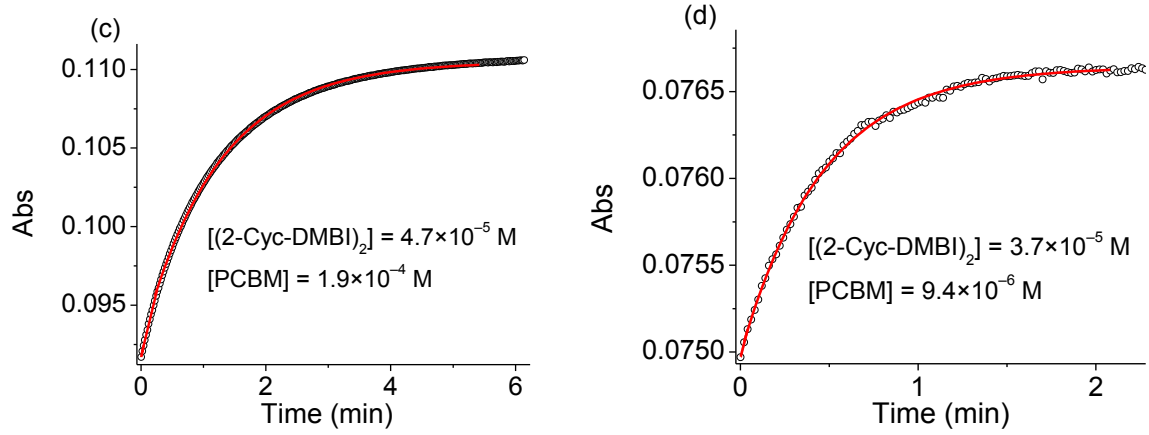

Figure S15. (a) Absorbance at 745 nm vs. time for the reaction of PCBM and (2-Cyc-DMBI)$_2$ with (2-Cyc-DMBI)$_2$ as the limiting reagent. The solid red line is the fitted first-order reaction curve. (b) Absorbance at 745 nm vs. time for the same reaction with PCBM as the limiting reagent. The solid red line is the fitted first-order reaction curve.

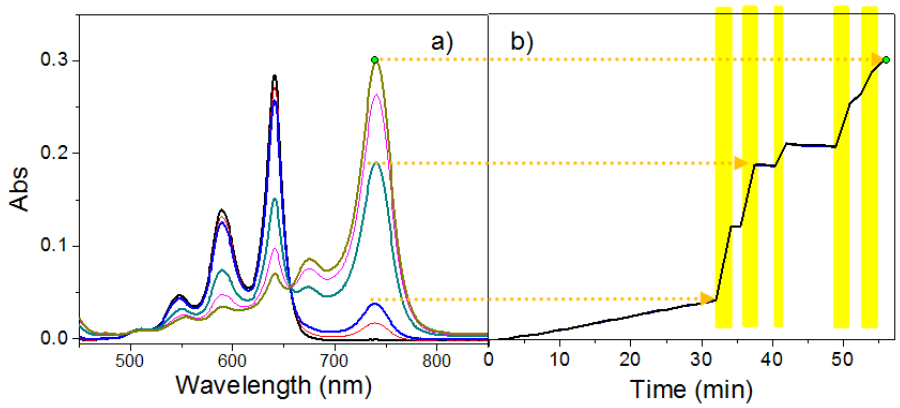

Figure S16. Evolution of spectra of a solution of $(2\text{-Rc-DMBI})_2$ (2×10^{-4} M) and TIPS Pentacene (2×10^{-4} M) in chlorobenzene in the dark and on exposure to laboratory light: a) shows spectra between 450-850 nm and b) shows normalized Absorbance at 745 nm vs. time with the yellow shading indicating the periods in which the samples were exposed to light.

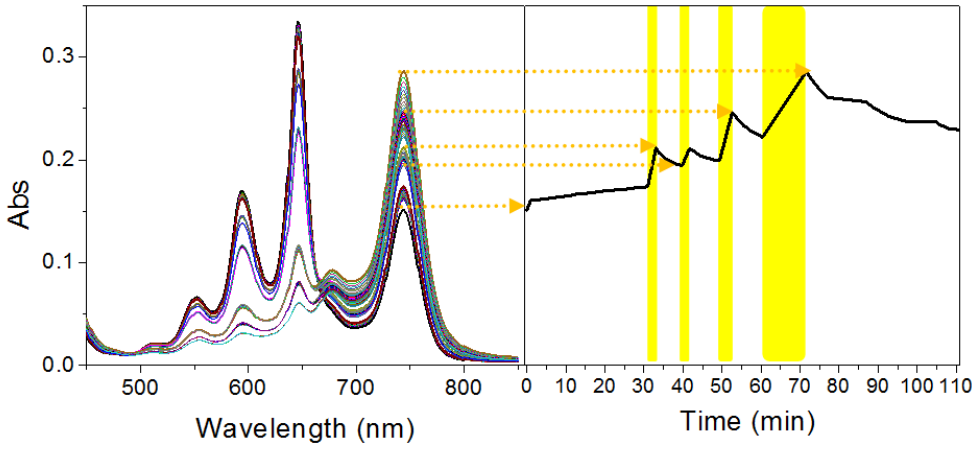

Figure S17. Evolution of spectra of a solution of $(2\text{-Cyc-DMBI})_2$ (2.6×10^{-4} M) and TIPSp (1.3×10^{-4} M) in chlorobenzene in the dark and on exposure to laboratory light: a) shows spectra between 450-850 nm and b) shows normalized Absorbance at 745 nm vs. time with the yellow shading indicating the periods in which the samples were exposed to light.

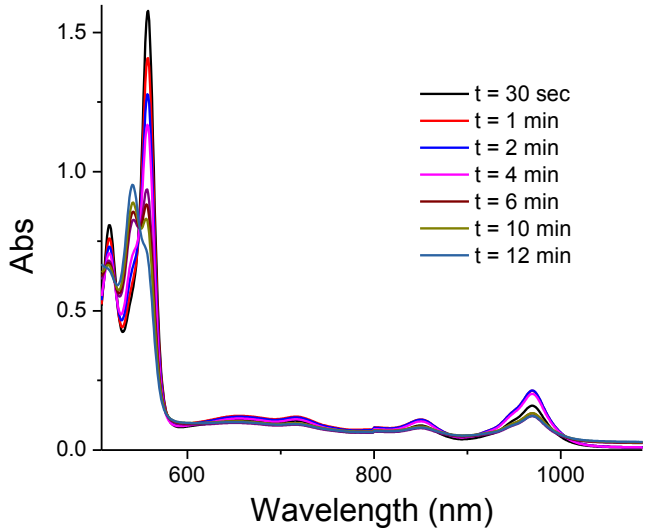

Figure S18. Vis-NIR spectra of a mixture of $(2\text{-Fc-DMBI})_2$ (1.45×10^{-4} M) and TES-ADT (2.90×10^{-4} M) in chlorobenzene.

10. References for Supporting Information

[1] B. D. Naab, S. Zhang, K. Vandewal, A. Salleo, S. Barlow, S. R. Marder, Z. Bao, *Adv. Mater.* **2014**, *26*, 4268.

[2] M. J. Frisch, G. W. Trucks, H. B. Schlegel, G. E. Scuseria, M. A. Robb, J. R. Cheeseman, G. Scalmani, V. Barone, B. Mennucci, G. A. Petersson, H. Nakatsuji, M. Caricato, X. Li, H. P. Hratchian, A. F. Izmaylov, J. Bloino, G. Zheng, J. L. Sonnenberg, M. Hada, M. Ehara, K. Toyota, R. Fukuda, J. Hasegawa, M. Ishida, T. Nakajima, Y. Honda, O. Kitao, H. Nakai, T. Vreven, J. A. Montgomery, J. E. Peralta, F. Ogliaro, M. Bearpark, J. J. Heyd, E. Brothers, K. N. Kudin, V. N. Staroverov, T. Keith, R. Kobayashi, J. Normand, K. Raghavachari, A. Rendell, J. C. Burant, S. S. Iyengar, J. Tomasi, M. Cossi, N. Rega, J. M. Millam, M. Klene, J. E. Knox, J. B. Cross, V. Bakken, C. Adamo, J. Jaramillo, R. Gomperts, R. E. Stratmann, O. Yazyev, A. J. Austin, R. Cammi, C. Pomelli, J. W. Ochterski, R. L. Martin, K. Morokuma, V. G. Zakrzewski, G. A. Voth, P. Salvador, J. J. Dannenberg, S. Dapprich, A. D. Daniels, O. Farkas, J. B. Foresman, J. V. Ortiz, J. Cioslowski, D. J. Fox in *Gaussian 09, Revision B.01*, Gaussian Inc.: Wallingford CT, **2010**..

[3] Y. Zhao, D. Truhlar, *Theor. Chem. Acc.* **2008**, *120*, 215.

[4] W. Koch, M. C. Holthausen, *A Chemist's Guide to Density Functional Theory*, Wiley & Sons, New York, **2000**.

[5] http://www.niehs.nih.gov/research/resources/software/tox-pharm/tools/index.cfm, accessed Apr 2015.

[6] A Lorentzian broadening was used for the spectrum shown in Figure 5; however, very similar spectra are obtained using a Gaussian broadening.